MICRO CRACK CHARACTERIZATION OF METAL MATRIX COMPOSITES BY 3D-REFRACTION-COMPUTED-TOMOGRAPHY

B.R. Mueller[1], A. Lange[1], M. Harwardt[1], M.P. Hentschel[1], B. Illerhaus[1], J. Goebbels[1], J. Bamberg[2], F. Heutling[2]
[1] BAM-Berlin, Berlin, Germany; [2] MTU Aero Engines, Munich, Germany

Abstract: For the first time Metal Matrix Composites have been investigated by 3D Computed Tomography combined with enhanced interface contrast due to X-ray refraction. X-ray refraction is a relatively new approach for the characterization of advanced materials. The related techniques of Refraction Topography and Refraction Computed Tomography have been developed and applied at our laboratory during the last decade to meet the actual demand for improved non-destructive characterization of high performance composites, ceramics and other low-density materials and components. X-ray refraction occurs, when X-rays crosses interfaces of spherical or cylindrical shape (e.g. pores or fibres) in the same way as visible light is refracted by lenses. These X-ray optical effects can be observed at small scattering angles of few minutes of arc as the refractive index n of X-rays is nearly unity ($n = 1 - 10^{-6}$). Due to the short X-ray wavelength of about 0.1 nm the technique determines the amount of inner surfaces and interfaces of nanometer dimensions. The technique is expected to solve many problems in understanding micro and sub micro structures in materials science. Applying 3D Refraction Computed Tomography some questions could be clarified for a better understanding of fatigue failure mechanisms under cyclic loading conditions.
The specimens for the test programme have been provided by MTU Aero Engines. They consist of a titanium matrix (Ti6242) reinforced by SiC fibres (SCS6). The investigations have been performed at the materials research station of BAM (BAM*line*) at the Synchrotron Facility BESSY in Berlin, Germany.

Introduction: The non-destructive characterization of high performance composites, ceramics and other advanced materials can be difficult. Anisotropy, heterogeneity and complex shapes reduce the performance of traditional non-destructive techniques, which have been optimized for isotropic single phase materials, preferably for metals.
The effect of X-ray refraction provides unconventional small angle X-ray scattering (SAXS) techniques which have been developed and applied in the last decade at our laboratory to meet the actual demand for improved non-destructive characterization of advanced materials. X-ray refraction reveals the inner surface and interface concentrations of nanometer dimensions due to the short X-ray wavelength near 0.1 nm. Sub-micron particle, crack and pore sizes are easily determined by "X-ray refractometry" without destroying the structure by cutting or polishing for microscopic techniques.

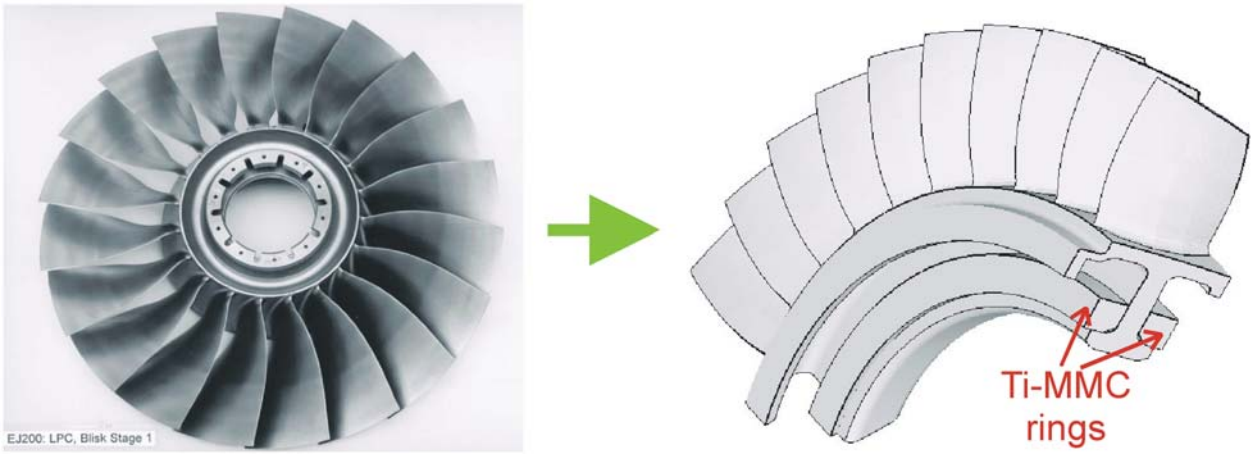

Figure 1: Bladed disk BLISK (left). Bladed ring BLING, larger hub bore diameter for new compressor designs; lower weight at same stiffness (rigth)

To enlarge the propulsive force of the next generation of aircraft engines some fundamental constructive changes has to be done. E.g. the design of the compressor section has to be changed from bladed disks (BLISK, Fig. 1 left) to bladed rings (BLING, Fig. 1 right) to archive a larger hub bore diameter for new compressor designs. This constructive changes presuppose new materials which have the same stiffness at a lower weight. Metal Matrix Composites (MMC) are basic materials based on metal alloys reinforced by ceramic fibres. These composites combine high tensile strength with low specific weight and are especially suited to be used in the compressor part of an aircraft engine. There mechanical properties are strongly influenced by the fibre orientation and the interface between the fibre and the matrix as well as the distribution of cracks and pores. While the orientation of the fibres is defined by the production process. The interfaces are also subjected to thermal and mechanical loading of the composite. Since several years titanium based alloy matrices reinforced by SiC fibres (Ti-MMC) are developed in the laboratories of the air and space industry. Used in aircraft engines they can reduce the weight of structural and functional components up to 50 %.

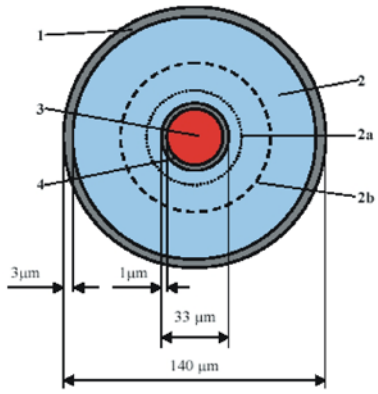

Figure 2: Assembly of the SCS6-fibre from Textron. 1: pyro-C-protectiv coating, 2: SiC, 3: C-fibre, 4: pyro-C-protectiv coating.

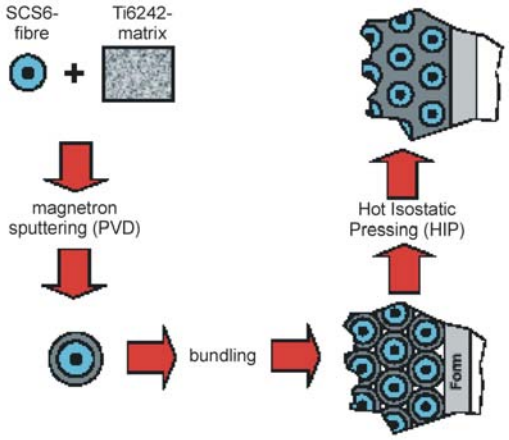

Figure 3: Procedure of Low Cycle Fatigue specimen manufacturing.

For a test programme cylindrical specimens have been provided by MTU Aero Engines. As reinforcing fibre the SCS6-fibre from Textron was taken. It has a 33 µm diameter carbon fibre as a core with a 1 µm pyro-C-protective coating, followed by SiC and again by a pyro-C-protective

coating of 3 µm (see Fig. 2). The overall diameter of the fibre measures 140 µm. The fibres were coated by magnetron sputtering with a 30 µm thick titanium base alloy Ti6242 and than bundled and formed by Hot Isostatic Pressing (HIP) (see Fig. 3). Static and cyclic forces were applied parallel to the fibre axis which leads to the evaluation of the mechanical parameters. After the mechanical tests the specimens were examined by metallographic methods and the fractured surfaces were analysed.

The manufacturing technology of Ti-MMC compounds is very challenging but the possibility of non-destructive inspection and characterization of these materials is up to now rather poor. As a new approach for non-destructive testing the specimens were investigated by 3D X-ray Refraction Computed Tomography as well. It is a promising tool to reveal the changes and development of the inter surfaces (e.g. fibre-matrix interface, cracks and pores) of those composites. The investigations should reveal whether the development of cracks and fibre failures after tensile load is distributed homogeneously across the sample, or locally concentrated.

The physics of X-ray refraction is quite similar to the well known refraction of the visible light by optical lenses and prisms, which is governed by Snell's law. However a major difference to the visible optics is, that the refractive index n of X-rays in matter is nearly one (1). This causes deflections at very small angles in the order of a few minutes of arc.

$$n = 1 - \varepsilon \qquad \text{with } \varepsilon \approx \rho \cdot \lambda^2 \text{ and } \varepsilon \cong 10^{-5} \text{ for glass at 8 keV radiation} \qquad [1]$$

ε is the real part of the complex index of refraction, ρ the electron density and λ the X-ray wavelength. In case of X-rays, where n < 1 the converging effect of convex lenses changes to divergence. Fig. 1 demonstrates the effect of small angle scattering by refraction of cylindrical lenses: A bundle of glass fibres with a diameter of 15 µm each as used for glass fibre reinforced plastics (GFRP) deflects collimated parallel X-rays within several minutes of arc. In fibres and spherical particles the deflection of X-rays occurs twice, when entering and when leaving the object (see magnification in Fig. 4). The oriented intensity distribution is collected by an X-ray film or a CCD camera while the straight (primary) beam is omitted by a beam stop. The shape of the intensity distribution of cylindrical objects is always the same even for very different materials, if the scattering angle is normalized to the "critical angle" θ_C of total reflection (see Fig. 5). This parameter depends only on the refractive index: $\theta_{2C} = 2\varepsilon$. The intensity of the deflected X-rays falls down to nearly zero at the critical angle of total reflection.

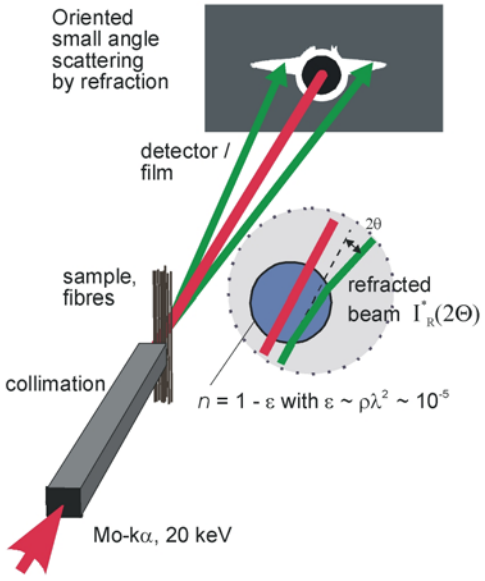

Figure 4: Effect of oriented small angle scattering by refraction of glass fibres.

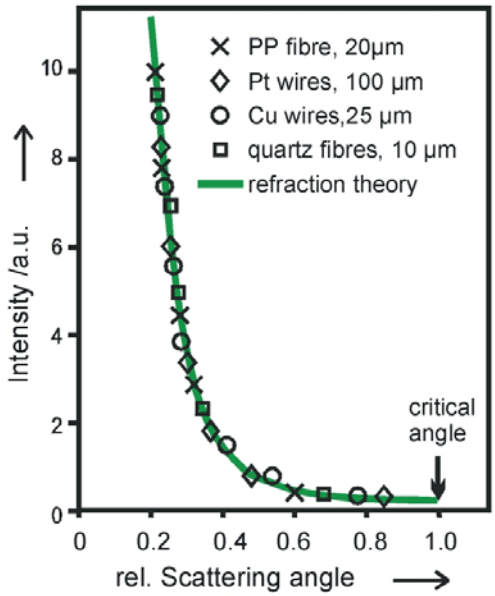

Figure 5: The normalized shape of the angular intensity distribution of cylindrical objects.

A cross section of 10^{-3} of the fibre diameter contributes to the detectable intensity above typically 2 minutes of arc. The effect of total reflection of X-rays occurs as well at the angle of grazing incidence but only 10^{-6} of the diameter is involved and therefore negligible. But well oriented planar surfaces can produce strong reflections. Based on Snell's Law the angular intensity distribution has been calculated and approximated for cylindrical fibres and spheres, as illustrated by Fig. 5. The refracted intensity of a cylinder without absorption effects can be expressed (2) as

$$I^*_R(2\theta') = \frac{J_0 \cdot 2R}{\varepsilon} \sin^3\left(\arctan\frac{\varepsilon}{\theta'}\right) = \frac{J_0 \cdot 2R \cdot \varepsilon^2}{\theta'^3} \qquad [2]$$

J_0 is the irradiation density of the incident X-ray beam onto the fibre, R is the radius of the fibre and $2\theta' = \theta$ is the scattering angle.

The SAXS instrumentation is relatively simple (see Fig. 6) but sometimes delicate in terms of its (thermo-) mechanical stability. It requires a collimated X-ray beam, a specimen manipulator, an X-ray refraction detector and a reference detector to monitor the specimen absorption and beam stability. The refraction intensity can be measured (3) according to Eq. 3.

$$I^*_R(2\theta') = I_R(2\theta') - I_{R0}(2\theta') \cdot \frac{I_A}{I_{A0}} = I_A \cdot k \cdot d \cdot N \cdot R \qquad [3]$$

I^*_R depends on the transmitted intensity I_A, the thickness d and the inner surface density $\Sigma = N \cdot R$ (N is the amount of fibres) of the specimen, respectively. The proportional factor k is a specific constant of the used apparatus and can be determined by measuring a probe with a known inner surface density. The proportional factor k and the inner surface density Σ define the refraction value $C = k \cdot \Sigma$, which is a relative measure of the surface density of the specimen. For practical measurements the refraction detector remains at a fixed scattering angle $2\theta'$, so that the surface density of the specimen can be measured according to:

$$C = \frac{1}{d} \cdot \left(\frac{I_R \cdot I_{A0}}{I_{R0} \cdot I_A} - 1\right) \qquad [4]$$

The conventional understanding of "continuous" small angle X-ray scattering (SAXS) is governed by the interpretation of diffraction effects. Apart from Guinier's theory for separated particles Porod explains diffraction of densely packed colloids (4) similar to Eq. 3. However both deal with particles two orders of magnitude smaller.

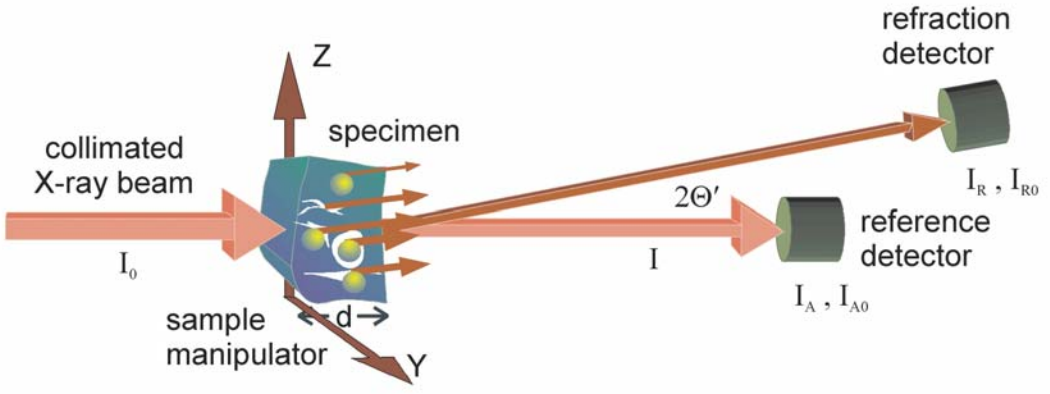

Figure 6: Basic principle of a SAXS instrumentation with collimated X-ray beam, specimen manipulator, a refraction detector, which measures the refracted intensity I_R of the specimen or I_{R0} if the specimen is not in place and a reference detector, which measures the intensity I_{A0} (without specimen) or I_A (with specimen), respectively.

A model composite has been made (see sketch in Fig. 7 on the left) in order to demonstrate the refraction behaviour of a bonded and debonded 140 µm sapphire fibre in a wax matrix. As shown in Fig. 6 the computer controlled manipulator system moves the model composite across the collimated X-ray beam. At each step the transmitted and refracted intensity is measured by the appropriate detector. The intensity values are stored in a matrix and visualized as a 2D topograph as shown in Fig. 7 middle and right, respectively.

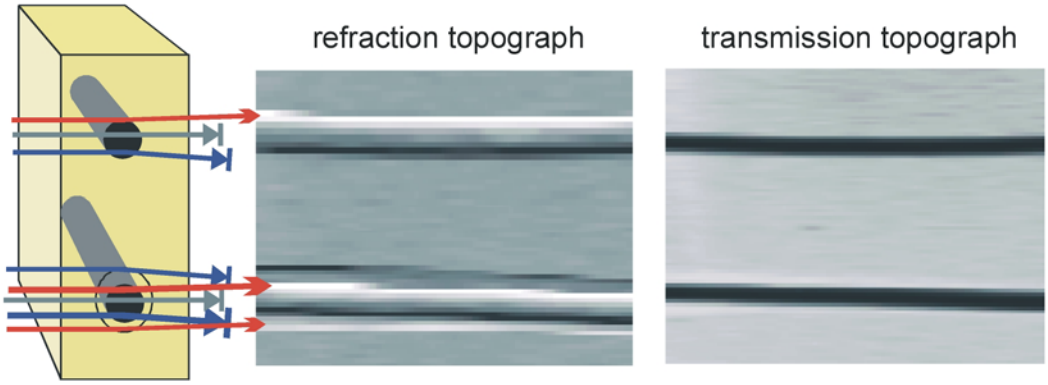

Figure 7: Model composite made of wax with a bonded (top) and debonded (bottom) 140 µm sapphire fibre (left). X-ray refraction at the interface of the bonded (top) and debonded (bottom) fibre (middle). X-ray transmission topograph of the model composite (right).

The right part of Fig. 4 shows the intensity distribution due to X-ray absorption of the model composite.
A dark-grey area means a strong absorption (mainly by the sapphire fibre) while a light-grey area means a weak absorption (mainly by the wax matrix). A difference between the bonded (top) and the debonded fibre (bottom) is not observably. In contrast the refraction topograph (middle part of Fig. 7) shows the resulting intensity distribution due to X-ray refraction. The bright horizontal stripe means a high refraction intensity caused by the sapphire-wax interface along the fibre of the model composite. The bonded fibre (top) is less contrasted compared to the debonded fibre (bottom) in the matrix. This is caused by the large density difference (high index of refraction) at the fibre-air interface and the matrix-air interface (bottom) in comparison to the minor density difference (low index of refraction) at the fiber-matrix interface of the bonded fibre (top).

Results: In our laboratory we have employed conventional X-ray tubes, crystallographic small angle scattering cameras and scintillation counters, respectively. The specimens where scanned or rotated across a single beam under pre selected fixed scattering conditions in order to receive spatial resolution. However the measurements are relatively time consuming and due to low X-ray energies from characteristic radiation of Cu- and Mo-anodes restricted to low density materials. Most of these disadvantages have overcome by use of synchrotron radiation. At the Berliner Electron Storage Ring for Synchrotron Radiation (BESSY) the Federal Institute for Materials Research and testing (BAM) has build up a hard X-ray laboratory (BAM*line*) for materials research (5). The usable photon energy range of the BAM*line* extends from 5 keV up to 80 keV for monochromatic radiation. The main advantages of Synchrotron Radiation are the high photon flux, the continuous energy range and the highly collimated and parallel photon beam, respectively. With the help of a monochromator system the appropriate photon energy can be chosen for the investigations. The experimental set up is sketched in Fig. 8. A parallel and monochromatic beam with a band width of about 2% is delivered by a Double-Multilayer-Monochromator (DMM). For a good transparency of the specimen we used a photon energy of 50 keV. The beam has a horizontal width of up to 30mm and a vertical width of a few

millimetres, respectively. The beam from the DMM is than reflected by two Si(111) single crystals in a symmetric configuration which are mounted on a 6-circle-goniometer. The crystals are set to there Bragg condition to reflect the chosen energy. An X-ray sensitive CCD-camera is placed behind the second crystal. It detects the photons reflected by the second crystal with a lateral resolution of about 5,3 x 5,3 μm^2.
Different from the set up for phase contrast CT, the sample is situated in the X-ray beam between the two crystals. The highly collimated and monochromatised beam from the first crystal transmits the specimen and will be attenuated according to the absorption properties of the specimen. Additionally, X-rays are deflected due to the refraction effect at all interfaces in the composite as explained above. This procreates a beam divergence which can be visualised by measuring the Rocking curve of the second crystal against the first crystal, with the

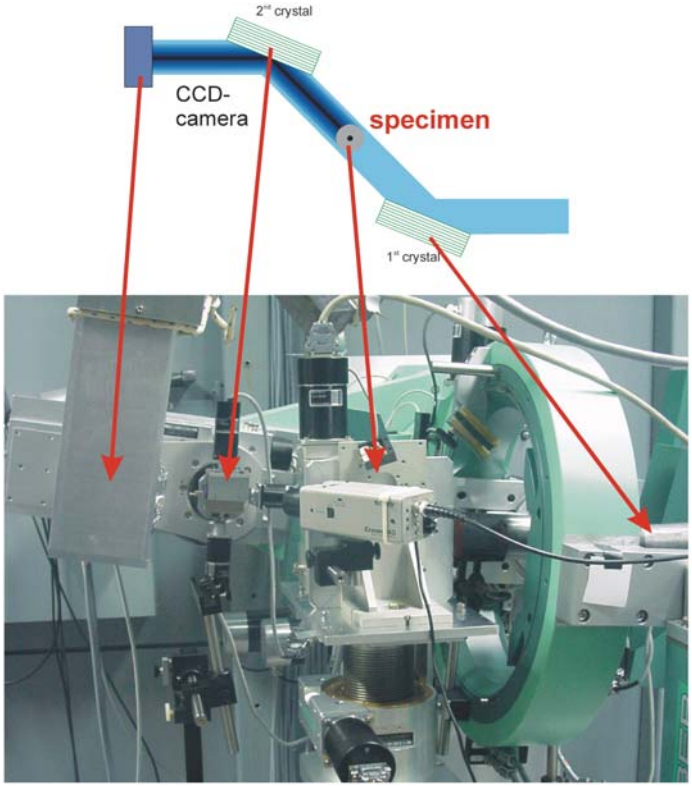

Figure 8: Sketch and photograph of the experimental set up at the BAM*line*

specimen (filled squares) and without the specimen (stars) between the two crystals, respectively. In the first case the Rocking curve width was broadened to FWHM = 1,8 arc seconds while the width in the last configuration was measured to be FWHM = 1,4 arc seconds (see Fig. 9). As a consequence only the attenuated and parallel X-rays are reflected by the second crystal and can enter into the CCD-camera if the crystal is set to the maximum of the rocking curve, as has be done in the measurements. Al refracted X-rays are missing at the CCD-camera and leads to an additional interface contrast in the topograph.

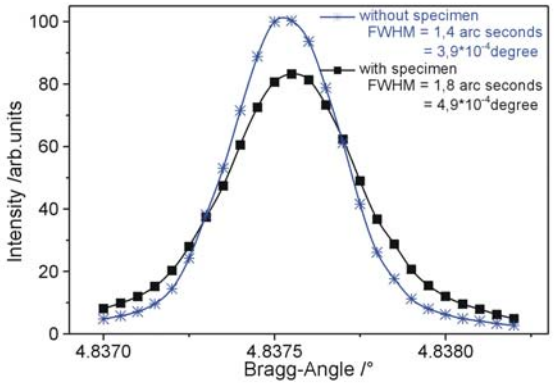

Figure 9: Rocking curve of the Si(111) single crystal pair in symmetric configuration from Fig. 8; with specimen (filled square) and without specimen (star) between the two crystals. The area under the curves is set to equal.

Discussion: Although two-dimensional refraction topography provides an effective new probe for analysing meso-structures of all kinds of heterogeneous materials, it is sometimes interesting to have section images of transversal resolution as known from X-ray computed tomography in order to overcome the overlap of details by projection effects. The measurements were performed by rotating the specimens around there cylindrical symmetry axis for 360 degrees in steps of 1 degree. After each step an exposure was taken. The data sets were analyzed by filtered back projection as known from the data treatments for conventional absorption CT.

Fig. 10 (left) shows the reconstruction (light-grey means strong absorption while dark-grey means less absorption) of one plane out of 300 planes of the absorption data set, which was taken in our CT-laboratory (100 kV, 4,7 x 4,7 x 4,7 μm^3 Voxel) at BAM. It shows the cross section of a low cycle fatigue specimen (LCP). The reinforcing SiC-fibres are shown up as dark discs with a slightly darker core. They are not symmetrically arranged to the rotational axis of the specimen. A crack (dark area) can be realised in the right part of the cross-section, which corresponds very well with the visible crack at the cladding of the specimen. No further indications can be seen for cracks or fibre failure in the remaining area.

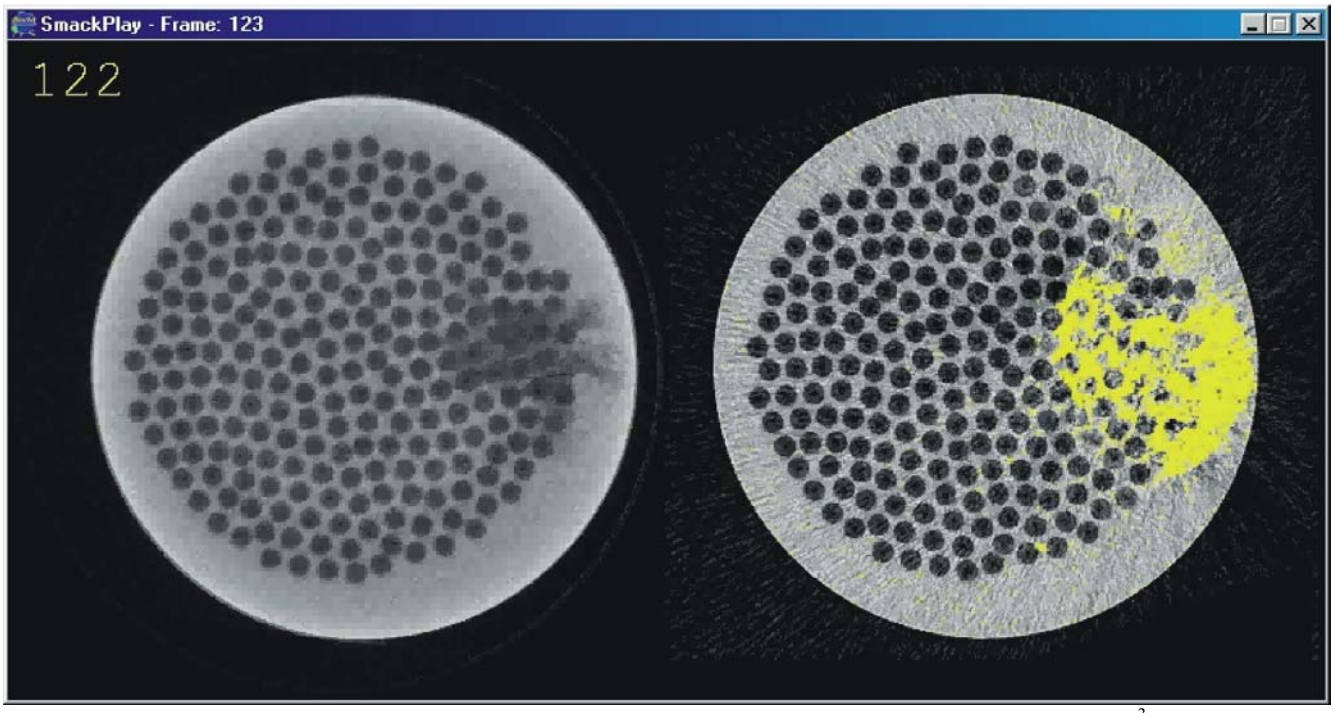

Figure 10: (left) Reconstruction of the absorption measurement; 100 kV, 4,7 x 4,7 x 4,7 µm^3 Voxel. (right) Reconstruction of the refraction measurement; 50 keV, 5,3 x 5,3 x 5,3 µm^3 Voxel; Specimen between the two crystals.

The right part of Fig. 10 demonstrates the feasibility of X-ray refraction computed tomography performed at the BAM*line* (50 keV, 5,3 x 5,3 x 5,3 µm^3 Voxel). It shows the same part of the specimen as the left side does, but even if the filtered back projection and the reconstruction is not jet adapted to the refraction effect, the information content is much higher. The absorption information is the same, but in addition the refraction effect reveal, that the crack distribution in the matrix (yellow coloured areas) is much broader than expected from the absorption information. To intensify the visualisation of single fibre failures and matrix cracks we subtracted one reconstructed plane, which was obviously not damaged from al the other planes. Fig. 11 shows the result of the image processing for one plane in the immediate vicinity of the plane shown in Fig. 10. All fibre failures in the reconstructed plane crop up as light-grey discs. The matrix cracks appear as grey areas. The deviation of the fibre positions with respect to the reference plane show up as a grey half-moon. All other areas which are not different form the reference plane are black. The outer shape of the specimen is marked by a red circle.

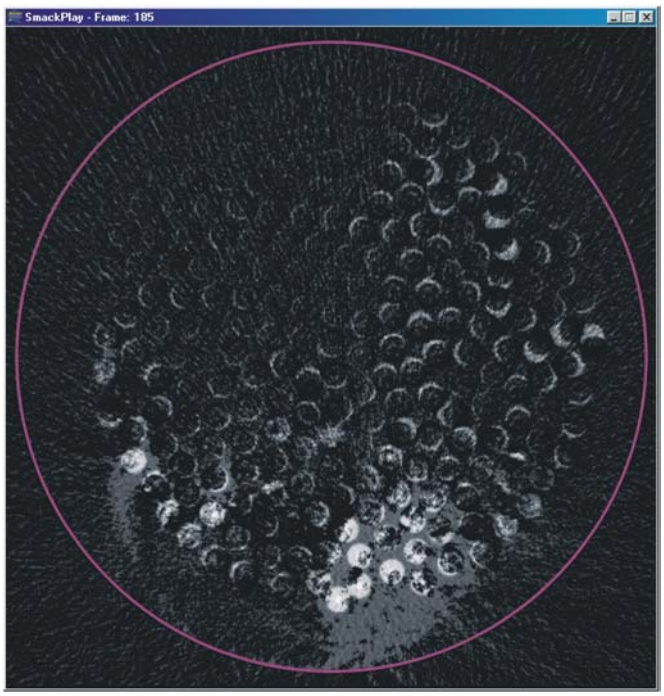

Figure 12: Reconstruction difference of a plane with single fibre failure and matrix cracks to a plane without failures.

Conclusions: X-ray refraction techniques combine analytical capabilities of sub-micrometer structure detection with the requirements of non-destructive full volume characterization. Its potential of contrasting cracks and pores will be an alternative to other attempts on raising the spatial resolution of CT machines. X-ray refraction therefore might help faster materials development, better understanding of meso-structures and partly replace micro analysis and mechanical testing in advanced materials science.

References:

(1) A. H. Compton, S.K. Allison, X-ray in Theory and Experiment, Macmillan and Co. Ltd., London, 1935.
(2) M.P. Hentschel, R. Hosemann, A. Lange, B. Uther, R. Brückner, Acta Cryst. **A 43**, 506 (1987).
(3) M.P. Hentschel, K.-W. Harbich, A. Lange, NDT&E International **27**, 275 (1994).
(4) G. Porod, Kolloid.-Z. **124**, 83 (1951).
(5) W. Görner, M.P. Hentschel, B.R. Müller, H. Riesemeier, M. Krumray, G. Ulm, W. Diete, U. Klein, R. Frahm, Nuclear Instruments and Methodes in Physics Researche **A467-468** 703 (2001)